Nanoscale

PAPER

View Article Online
View Journal | View Issue

Cite this: *Nanoscale*, 2023, **15**, 17473

Facile microfluidic synthesis of monodispersed size-controllable quantum dot (QD) microbeads using custom developed QD photoresist†

Byeongseok Kim,‡[a] Samir Kumar,‡[a] Bumsoo Chon,[b] Ho-Jin Son,[b] Sang Ook Kang[b] and Sungkyu Seo*[a]

Fluorescent microbeads (MBs) are widely used as next-generation biosensors for the detection of target chemicals at highly sensitive concentrations, and for imaging and tracking *in vitro* and *in vivo*. However, most known methods for producing fluorescent MBs require complicated multistep processes that result in low production rates. In this study, we report a method for fabricating micrometer-sized quantum dot microbeads (QD-MBs) using a microfluidic chip and specially designed QD photoresist (QD-PR). This on-demand lab-on-a-chip method yielded monodispersed QD-MBs ranging from 1.89 to 33 μm with a coefficient of variation of less than 10%. The size distribution of the fabricated QD-MBs was Gaussian with a peak around the mean diameter and a spread of sizes around the peak. Compared with nanoscale QDs, the fabricated QD-MBs showed no emission loss. The full-width at half-maximum of the emission peak of the QD-MBs was smaller than that of the colloidal QDs, indicating a more uniform distribution and a higher density of QDs within the MB structure. In addition, we investigated the microfluidic flow regime that yielded the most uniform and controllable QD-MB. The MBs in the dripping regime were spherical and monodisperse, with an excellent particle size distribution. In this study, we present a simple and effective strategy for producing QD-MBs with controllable sizes, which can be crucial in diverse fields such as biosensing, drug delivery, and imaging.

Received 20th July 2023,
Accepted 16th October 2023

DOI: 10.1039/d3nr03544a

rsc.li/nanoscale

Introduction

Biosensors have revolutionized the diagnosis and monitoring of diseases, enabling onsite, rapid, and accurate detection of biomarkers.[1–3] Recently, fluorescent microbeads (MBs) have emerged as an emerging tool for various biosensing applications, such as detection of nucleic acids,[4] proteins,[5] bacteria,[6] circulating tumor cells,[7,8] and point-of-care testing (POCT).[9,10] Fluorescent MBs have a large surface-to-volume ratio, which allows for a simple and efficient method of probe immobilization, resulting in sensitive detection, which is widely used in POCT.[7,11] Moreover, fluorescent MBs also enable multiplex detection, allowing simultaneous detection of multiple analytes. These fluorescent MBs can be manufactured from a variety of materials, such as polymers[12] and silica,[13] with different sizes, shapes, and surface functionalizations.[14–16] Organic dyes are the most widely used fluorescent materials for the fabrication of fluorescent MBs.[17–19] Fluorescent organic dyes are inexpensive and have high quantum yield, but they suffer from photobleaching, spectral overlap, and require multiple excitation sources. Quantum dots (QDs), on the other hand, overcome these limitations of organic dyes and have high photostability, narrow and tunable emission spectra, and multiple QDs can be excited with a single wavelength.[20–23]

There are three main strategies for the preparation of fluorescent MBs: encapsulation, decoration, and *in situ* embedding of fluorescent materials.[18,24,25] In the encapsulation method, fluorescent materials such as organic dyes or QDs are embedded in a polymer matrix such as polystyrene.[26] The fluorescent nanoparticles inside the MBs are encapsulated by diffusion permeation based on solvent concentration gradients, resulting in swelling of the MBs. Encapsulation can protect fluorescent materials from environmental factors such as pH and temperature, but it can also reduce their quantum yield (QY) and brightness.[27] To prevent aggregation and ensure successful encapsulation, it is also important to ensure that the nanoparticles introduced into the MBs are compatible

[a]*Department of Electronics and Information Engineering, Korea University, Sejong 30019, Republic of Korea. E-mail: sseo@korea.ac.kr*
[b]*Department of Advanced Materials Chemistry, Korea University, Sejong 30019, Republic of Korea*

†Electronic supplementary information (ESI) available. See DOI: https://doi.org/10.1039/d3nr03544a

‡These authors contributed equally.

with the solvent used and have a size that matches the pores of the MBs. Although this method enables one-pot synthesis of fluorescent MBs, it is challenging to control the morphology and size of the MB produced.[28] In the decoration method, fluorescent materials are attached to the surface of the MBs using a layer-by-layer method. Charged fluorescent nanoparticles and oppositely charged polyelectrolytes are applied in alternating layers.[29,30] By controlling the number of layers applied, the resulting fluorescent MBs could have a uniform coating of nanoparticles and different fluorescence intensities. Decoration can increase the fluorescence intensity and stability of MBs but can also lead to nonspecific binding and aggregation. In addition, this method is time-consuming and labor-intensive because each step requires multiple washes of the nanoparticles and polyelectrolytes, and there is a possibility that fluorescent nanoparticles may leak from the surface of the MBs.[18] In *in situ* embedding, fluorescent materials are incorporated during the synthesis of MBs by polymerization or emulsification and solvent evaporation.[31,32] In these methods, the size of the fluorescent MBs can be tuned by adjusting the concentration of the precursor and the mixing rate.[33] However, complex synthesis conditions and purification steps may also be required. In addition, the MBs produced by these techniques are highly polydisperse, which affects the efficiency and reliability of bioassays.[34]

In recent years, microfluidic techniques have been used to produce MBs with a smaller size distribution and greater stability.[35,36] In microfluidic methods, droplets are produced by the controlled flow of two immiscible fluids (such as oil and water) through a microfluidic channel with a narrow constriction or junction.[37] The flow rate and channel geometry can be precisely controlled to produce droplets with a narrow size distribution and accuracy and can be easily integrated with other technologies such as sensors, detectors, and imaging systems.[38–41] This integration allows real-time monitoring and analysis. Several recent reports have demonstrated the microfluidic synthesis of QD microbeads (QD-MBs).[42–44] However, the fabrication methods used in these studies are complex and involve multistep processes that limit scalability, reproducibility, and cost-effectiveness. For example, Liu *et al.* proposed a microfluidic strategy for the fabrication of monodisperse fluorescent QD-embedded alginate barcodes.[45] However, researchers were only able to fabricate QD-MBs of a single size (46 μm). Kim *et al.* fabricated QD-MBs capable of single-peak laser emission in a microfluidic glass chip using an oil-in-water emulsion.[33] However, after fabricating the QD-MBs, crosslinking was performed by ligand exchange, which is a complex, multistep process that requires a specialist. In addition, the diameter of the QD microdroplets in the oil phase decreased by 72% after drying, which made it difficult to accurately control the on-demand production of QD-MBs of different sizes.

In this study, we describe a simple on-demand method for fabricating uniform and size-controllable QD-MBs using a specially designed QD photoresist (QD-PR) and microfluidic devices. These QD-MBs were fabricated and cured in a single step in a microfluidic chip using a specially designed photoresist, that is, the supercoater. The size of the QD-MBs was effectively controlled by adjusting the flow rates of the continuous and dispersed phases during the fabrication. The QD-MBs were characterized by fluorescence microscopy, and their size distribution and full-width at half-maximum (FWHM) were analyzed. In addition, we analyzed the microfluidic droplet regime suitable for the preparation of QD-MBs with uniform and controllable sizes. The proposed technology combines QDs with microfluidics, and offers excellent optical properties and potential for biosensing applications.

Experimental section

Preparation of the QD photoresist

In this study, a custom-made photocurable ceramer composite called QD-PR, which is a composite of QDs and a specially developed super-coater, was used to fabricate QD-MBs (see Fig. 1a and b).[46] The super-coater consists of several functional components: (1) inorganic dispersant: colloidal silica serves as an inorganic dispersant and prevents interactions between the added QDs. (2) Surface passivator: 3-methacryloxypropyltrimethoxysilane (A-174), a monofunctional acrylate, acts as the surface passivator. It binds the heterogeneous insulator (colloidal silica) and improves its compatibility with other alkoxy acrylates. (3) Photocuring resins: this category includes several polyfunctional alkoxy acrylates, namely dipentaerythritol penta/hexa acrylate (DPPA/DPHA), pentaerythritol triacrylate (PETA), and 4-acryloylmorpholine (ACMO), and (4) a photoinitiator, namely 1-hydroxycyclohexylphenyl ketone.

The supercoater was prepared by heating and stirring 8 wt% DPPA/DPHA, 56 wt% PETA, 16 wt% colloidal silica, 10 wt% A-174, and 10 wt% ACMO. The mixture was vacuum-distilled at 52 ± 2 °C. for 2 h to remove most of the water/methanol solution and obtain the super-coater. DPPA/DPHA was purchased from Sigma-Aldrich (Massachusetts, USA), PETA stabilized with 300–400 ppm 4-methoxyphenol, A-174 from Alfa Aesar (Massachusetts, USA), ACMO stabilized with MEHQ, and 1-hydroxycyclohexyl phenyl ketone from Tokyo Chemical Industry Co., Ltd (Tokyo, Japan). Core–shell CdSe/ZnS QDs (5 mg mL^{-1}) with an emission peak at 625 nm were purchased from Dong-A Carbon Tech (Chilgok, Republic of Korea).

Using QD-PR, MBs were fabricated using microfluidic technology. This process involves the direct exposure and curing of the fabricated QD-MBs. During exposure, the photoactive compound in the supercoater emits free electrons from the exposed area, initiating the bonding and curing of the acrylates. As the QDs were dispersed in the supercoater, they were enclosed by the cured supercoater, resulting in the formation of solidified QD-MBs.

In our study, we specifically used a custom photoresist formulation to prepare the QD-MB. Commercially available photoresists are used in various fabrication processes. If commercially available photoresists are used, it is necessary to investigate factors such as the compatibility of QDs and their

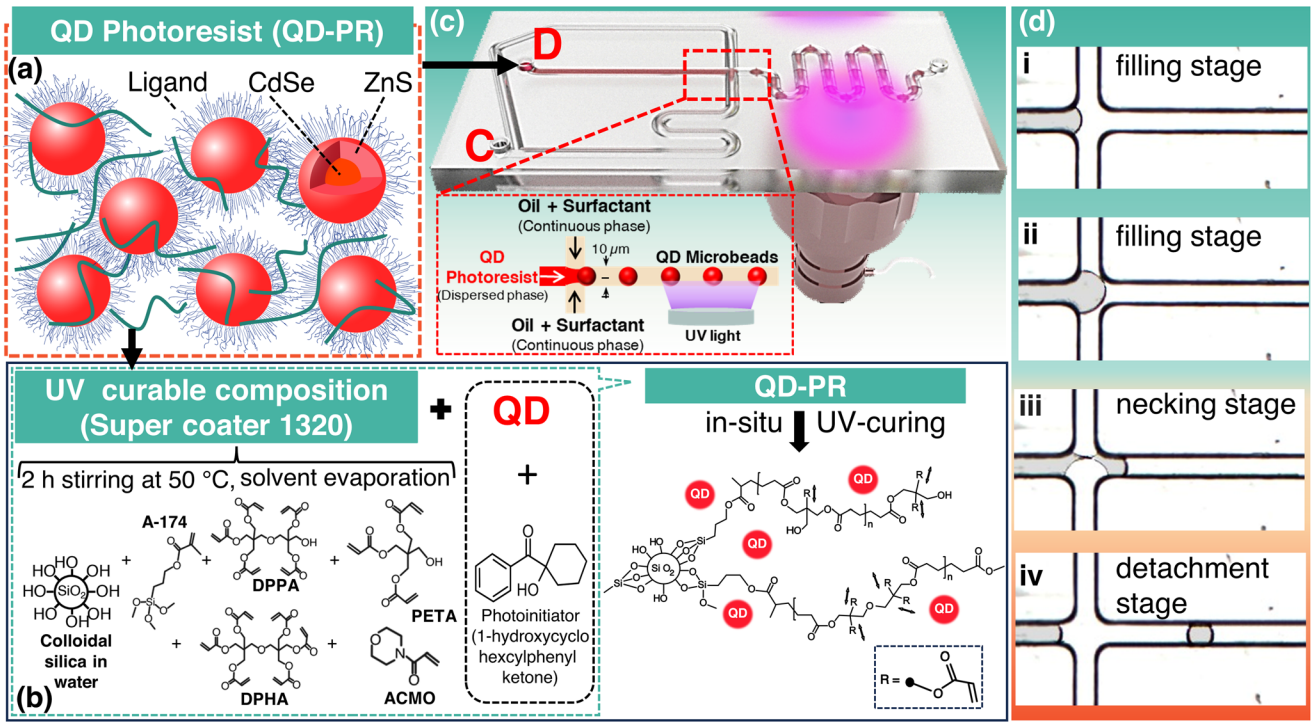

Fig. 1 (a) Schematic representation of QD-PR, which is the final blend of CdSe/ZnS QD and supercoater. (b) Schematic representation of the material composition for the synthesis of the specially designed UV curable creamer composite, supercoater (c) schematic representation of the proposed lab-on-a-chip microfluidic technology for QD-MB generation and UV exposure zone with serpentine channel for curing QD-MBs. (d) Sequential snapshots of the droplet formation stages—filling stage (i and ii), necking stage (iii), and detachment stage (iv)—of droplet generation in a microfluidic chip.

ability to adequately encapsulate them. Additionally, because we employed a microfluidic method to fabricate the QD-MBs, the viscosity of the photoresist also plays a crucial role in achieving uniform QD-MBs. Furthermore, the chemical composition of the photoresist and curing mechanism must preserve the properties and dispersion of QDs.

In contrast to commercially available photoresists, our super-coater consists of colloidal silica, which serves as an inorganic dispersant, and various alkoxy photocuring acrylates. Colloidal silica not only has insulating properties but also prevents electronic interactions between the added QDs and provides geometric separation. In addition, the viscosity of the super-coater can be precisely adjusted by controlling the relative proportions of the three alkoxy acrylates (DPPA, DPHA, and PETA), each with different lengths and shapes of alkoxyl chains. The customized properties of our supercoater offer advantages that make it ideal for the production of highly dispersed uniform QD-MBs using microfluidics.

Microfluidic devices

The microfluidic device used to fabricate the QD-MBs consists of two parts, as shown in Fig. 1c. A nozzle was used to disperse the QD-PR droplets and ultraviolet (UV) light exposure part of the *in situ* photopolymerization to cure the MBs. Polycarbonate microfluidic chips with hydrophobic surfaces were purchased from Microfluidic ChipShop (Jena, Germany). The beads were generated by pouring a dispersed phase (QD-PR) into the central channel and pumping a continuous phase (oil solution) into both channels at a constant flow rate to generate a shear force (Fig. 1c). Fig. 1d illustrates the successive stages—the filling stage (Fig. 1d(i and ii)), necking stage (Fig. 1d(iii)), and detachment stage (Fig. 1d(iv))—of droplet generation in a microfluidic chip. The microfluidic channel had a height and width of 10 μm.

Preparation of the QD microbeads

Inlet "D" was used to introduce the dispersed phase into the microfluidic device, while inlet "C" was used to inject the continuous phase with a syringe pump. The dispersed and continuous phases were introduced into the microfluidic device through a Tygon tube (inner diameter 1.59 mm), and the flow rates were controlled using syringe pumps (NE-1000, New Era Pump Systems, Inc., NY, USA). The size of QD-MBs can be tuned by adjusting the flow rate. The flow rate of the dispersed phase was varied from 0.3 to 0.9 μL h^{-1}. Silicone oil (KF-96, 3000 cs, Shin-Etsu Chemical Co. Ltd, Tokyo, Japan) with 4 wt% of a mixture of surfactants (Span 80 and Tween 80; Samchun Chemical Co., Ltd, Seoul, Republic of Korea) was used for the outer continuous phase. A combination of Span 80 and Tween 80 surfactants was used to achieve the desired balance between hydrophilicity and lipophilicity (HLB). Monodisperse QD-MBs were prepared by photopolymerization of QD-PR

in situ for less than 1 s using a UV lamp (365 nm, M365L2, Thorlabs) (Fig. 1c). A high-speed camera (VC-3MC, Vieworks) was used to monitor the MBs during the process. After the formation of the QD-MBs, they were collected in a reservoir and dispersed in oil. The oil was removed by centrifugation, followed by the removal of all liquids except the QD-MBs using a pipette. To ensure the complete removal of the oil, the cured QD-MBs were washed several times with deionized water before further use.

Characterization

Fluorescence images of QD-MBs were acquired using a fluorescence microscope (TCM400, Labomed, Fisher Scientific, KS, U.S.A.) and a digital color camera (PAXcam2+, PAX-it, IL, U.S.A.). The average size and coefficient of variation (CV) of the MBs were determined by analyzing at least 200 particles in each image using image analysis software (ImageJ2).[47] The coefficient of variation (CV) was calculated using the following equation.

$$\mathrm{CV}(\%) = \frac{\text{Standard deviation}}{\text{Mean QD microbead diameter}} \times 100 \qquad (1)$$

The fluorescence spectra of the QD-MBs were analyzed using a confocal spectrofluorometer (ACRON, UniNanoTech, Yongin, Republic of Korea).

Results and discussion

The aim of this study is to develop a simple and efficient method for producing uniform and size-controllable QD-MBs. To fabricate QD-MBs, we first embedded QDs in a photosensitive material called super-coater. The super-coater was then shaped into MBs using microfluidics and irradiated with UV light to solidify and entrap the QDs. The photoactive compound in the photoresist emits free electrons upon UV irradiation, causing the acrylates to bind and cure. The QDs dispersed in the photoresist are then trapped between the cured layers of the super-coater, forming QD-MBs. The dispersion of QDs can also affect the stability of QD-MBs performance. If the QDs are not uniformly dispersed, they may aggregate more easily and degrade QD-MBs. In our previous study, we examined the dispersion of QDs in a super-coater used to fabricate QD-MBs. Fluorescence microscopy and image analysis confirmed that the QDs were uniformly dispersed in SC1320 and SC1230 super-coaters (Fig. S1, ESI†). This uniform dispersion is critical for the uniform performance of each QD-MB, as shown in Fig. 2(a–d). However, in this study, we used the SC1320 supercoater because its viscosity was suitable for producing QD beads using our microfluidic method. This uniform dispersion is crucial for consistent performance of each QD-MB, Fig. 2(a–d).

The QD-MBs were characterized using fluorescence microscopy, and their size distribution and FWHM were analyzed. Fig. 2(a–d) shows the fluorescence microscopy images of QD-MBs of different sizes (33.03–2.11 μm) obtained by varying the flow rates. The images were converted to 8-bit black-and-white images, and the MB size was automatically measured using ImageJ2. The results in Fig. 2(a–d) show the successful fabrication of QD-MBs of different sizes with a uniform and spherical shape and uniform emission. The size distribution of the fabricated QD-MBs in Fig. 2(a–d) and the FWHM, which

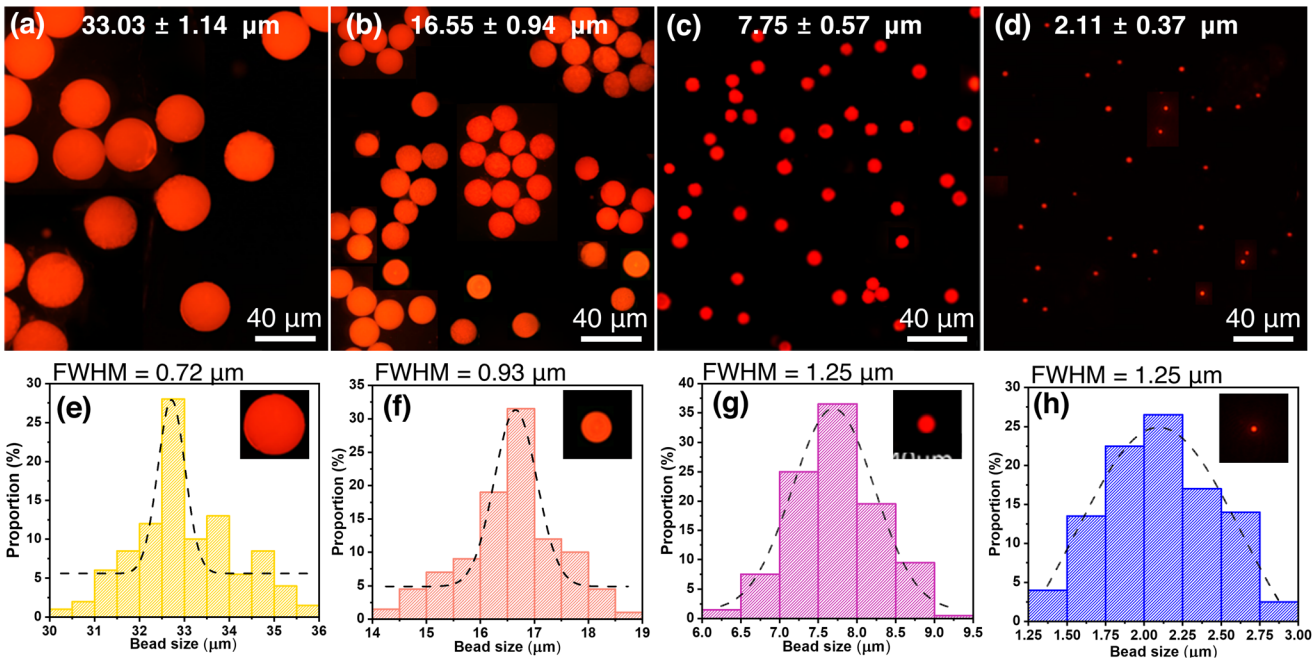

Fig. 2 Fluorescence micrographs and size distribution of QD-MBs of different sizes, depending on the flow rate. (a–d) Micrographs of QD-MBs with average diameters of 33.03 μm, 16.55 μm, 7.75 μm, and 2.11 μm, respectively. (e–h) Corresponding size distribution histograms of the QD-MBs.

is a measure of the particle distribution of the QD-MBs, are shown in Fig. 2(e–h). The size distribution curves in Fig. 2(e–h) appear to be Gaussian, with a peak around the mean diameter and a spread of sizes around this peak. The dotted line in each panel corresponds to a Gaussian distribution curve that best fits the size-distribution data. In Fig. 2(a–c), the CV is less than 10%, demonstrating the production of homogeneous QD-MBs. The CV value was minimum (3.5%) for the largest (33.03 μm) QD-MBs and maximum (17.5%) for the smallest (2.11 μm) QD-MBs. The smallest QD-MB has a higher CV because these are preliminary results obtained without optimizing the dispersed and continuous phase speeds, and microfluidic chips with different channel diameters were used for the smallest QD-MBs.

Fig. 3(a) shows a comparison between the fluorescence emission spectra of the QD-MBs and colloidal QDs. Fig. 3b and c show the photographs of the colloidal QD and QD-MB samples, respectively. The FWHM of the emission peak of QD-MB (21.2 nm) was smaller than that of the colloidal QDs (22.9 nm). The narrower FWHM of the QD-MBs indicates a more uniform distribution and higher density of QDs within the MB structure compared with the colloidal form of QDs. This observation is consistent with previous studies that have shown that the size and packing of QDs in a polymer matrix can significantly affect their optical properties such as fluorescence emission.[48] In addition, the improved uniformity and packing of QDs within the MB structure can improve the stability and reproducibility of the optical properties of QD-MB. This is because a more uniform distribution and higher density of QDs within the MBs could reduce the likelihood of aggregation or clustering of QDs, which are known to affect their optical properties. The potential relationship between the QD dispersion in QD-MBs and their QY could be due to the complicated phenomena of energy transfer and reabsorption. However, the exact relationship between the QD dispersion and QY in QD-MBs is complicated and requires further investigation. Although we did not directly investigate this relationship, we recognize its importance. In addition, in our previous research, we explored the effects of the QD concentration and super-coater film on the optical properties of QDs. We found that the QDs in the super-coater had a QY of 59.19%, which means that their optical properties were maintained even after the super-coater was cured.[46]

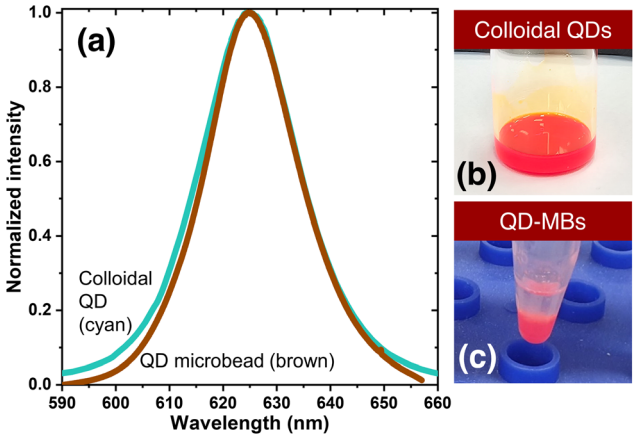

Fig. 3 (a) Comparison of the normalized fluorescence intensities of colloidal QDs and QD-MBs. Photographs of (b) colloidal QD and (c) QD-MB samples.

Next, we showed that the size of the QD-MBs can be precisely controlled by regulating the flow rates of the continuous and dispersed phases during production. The relationship between the QD-MB diameter and the flow rates for the dispersed flow rates between 0.3–0.9 μL h^{-1} is shown in Fig. 4. To investigate how the two flow rates affected the QD-MB size, we fixed the dispersed phase flow rate and changed the continuous flow rate. Our results show that both flow rates significantly affect the size of the QD-MBs. With a fixed value for the dispersed phase, an increase in the continuous flow rate

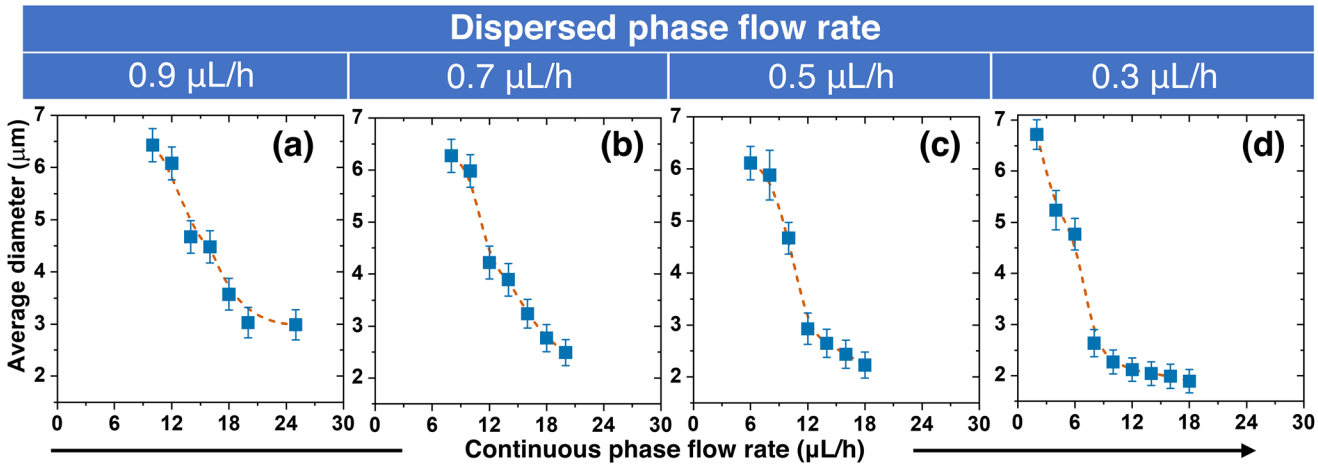

Fig. 4 Relationship between QD-MB diameter and continuous flow rates. The dispersed flow rate was set at 0.9 μL h^{-1} (a), 0.7 μL h^{-1} (b), 0.5 μL h^{-1} (c), and 0.3 μL h^{-1} (d). Increasing the continuous flow rate led to a decrease in the average diameter of QD-MBs. The coefficient of variance for the size distribution was less than 10%.

resulted in a decrease in QD-MB size. This could be because increasing the flow rate of the continuous phase (oil solution) results in smaller QD-MBs because of the high shear forces that break larger droplets into smaller ones.[49,50] Simultaneously, the size of the QD-MBs decreased as the flow rate of the dispersed phase decreased. At a continuous flow rate of 12 μL h^{-1}, the sizes of QD-MB at dispersed phase flow rates of 0.9 μL h^{-1}, 0.7 μL h^{-1}, 0.5 μL h^{-1}, and 0.3 μL h^{-1} were approximately 6.1 μm, 4.2 μm, 2.9 μm, and 2.1 μm, respectively. The CV was less than 10%, indicating the production of monodisperse beads. Decreasing the flow rate of the dispersed phase resulted in smaller QD-MBs because the volume of the photoresist in each droplet was smaller. In short, increasing the continuous flow rate results in a decrease in the size of the QD-MBs, whereas increasing the flow rate of the dispersed phase results in an increase in the size of the QD-MBs. Thus, to produce the smallest possible QD-MBs, a high continuous flow rate of the oil solution and low dispersed flow rate of the QD-PR are required. If the continuous flow rate is too high or the dispersed flow rate is too low, droplet formation is hindered, resulting in reflux without droplet formation. Therefore, a minimum dispersed flow rate of 0.3 μL h^{-1} was used in this study.

Furthermore, different flow rates resulted in different flow regimes and average bead-size distributions (Fig. 5). However, not all flow rates are proportional or inversely proportional to the size. If the flow rate is too low or too high, it results in a different flow regime. Four major flow regimes were observed during the experiment: dripping, jetting, elongation, and reflux. Among these, the dripping regime proved to be the best for the formation of stable beads. In the jetting and elongation regimes, unstable beads can form, and in the reflux regime, the fluid flows into the other channels because the flow rate on one side is too high.

In a T-junction microfluidic system, the dispersed phase enters the main channel and meets the continuous phase flow through the side channel. As a result, a pressure gradient forms across the developing droplet owing to the interaction between the viscous stresses and capillary pressure. When the pressure exceeds that within the tip of the dispersed phase, the interface between the two phases deforms and forms a neck. The neck eventually thins and breaks, leading to droplet formation (Fig. 5b(i)). The dripping regime is a shear-dominated process in which droplets form because of the local shear stresses. The dispersed fluid occupies only a part of the main channel diameter and is completely enclosed by the continuous phase.

In the jetting regime, a continuous jet of the dispersed phase forms at the junction (Fig. 5b(ii)). This occurs when the equilibrium between the viscous stresses and capillary pressure at high flow rates of both the continuous and dispersed phases favors jet formation over droplet formation. Typically, the droplets produced are smaller than the channel dimensions. However, because they are produced in the form of long droplets, when cured in this state, they cannot be rapidly discharged from the channel, resulting in clogging. In addition, the long droplet shape is unsuitable for bio-labeling because of its increased surface area.

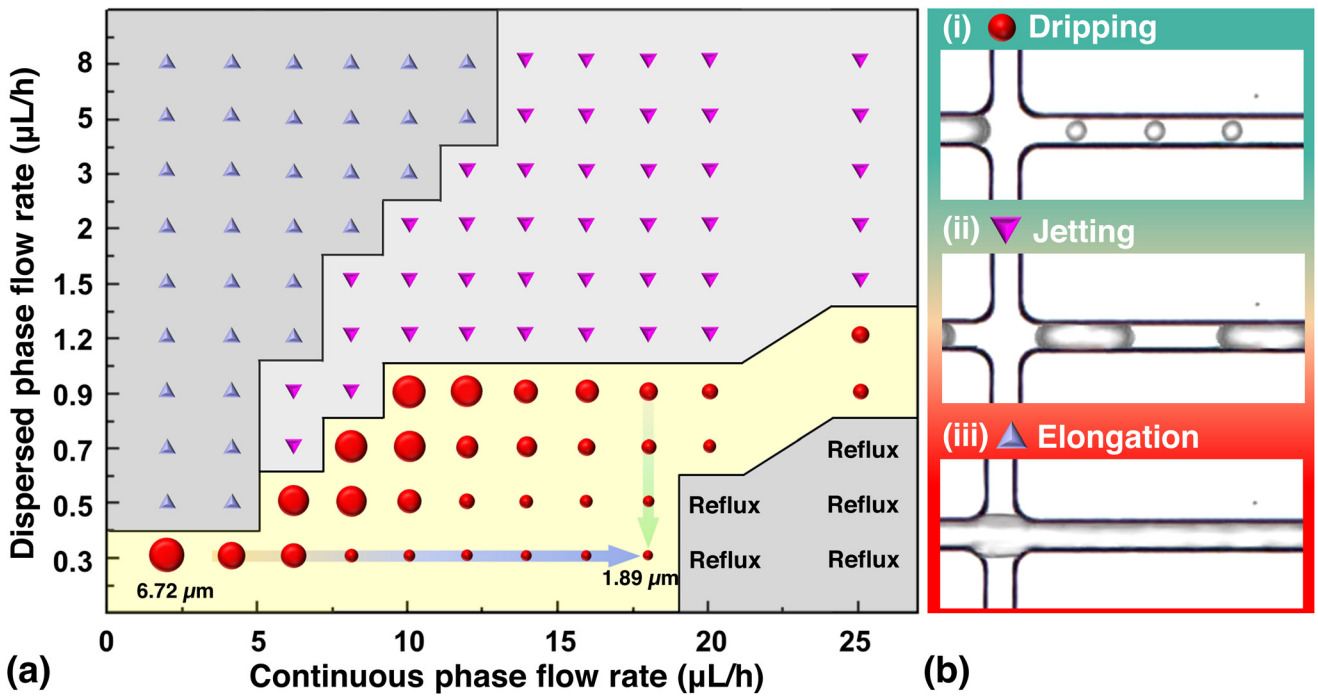

Fig. 5 Droplet generation and flow regimes observed in the microfluidic device. (a) Phase diagram showing flow regimes and bead sizes as a function of the flow rates of the dispersed and continuous phases. (b) Optical images of three different flow regimes in T-junction: (●) dripping, (▼) jetting, and (▲) elongation.

Elongation occurs when the dispersed phase forms long filaments or slugs instead of droplets or jets (Fig. 5b(iii)). When the high flow rate of the dispersed phase meets the low flow rate of the continuous phase, the shear force is not sufficient to break the dispersed phase; therefore, the droplet along the microchannel becomes a long cylindrical filament. These elongated filamentary liquids of the dispersed phase can cause clogging in the microchannels owing to their easy curing and long duration. Reflux occurs when the dispersed phase flows back into the inlet channel, instead of forming droplets or jets. This can occur if the continuous flow rate is remarkably high compared with the dispersed flow rate. The dripping method can be used to produce small beads. In contrast, the jetting and elongation methods, which form unstable droplets, cannot form a uniform sphere and may cause clogging in the channel, making them unsuitable for QD-MB production.

The transition from one regime to the other depends on the dimensionless capillary number (C_{ac}), which is the ratio of viscous force to capillary force—expressed as $C_{ac} = \mu_c U_c/\gamma$, and the ratio of flow rates Q_d/Q_c, where U_c is the characteristic velocity, ρ_c is the density, γ is the interfacial tension, and μ is the viscosity of the fluid in the continuous phase, and Q_c and Q_d are the flow rates of the continuous phase and disperse phase, respectively.[51] Since the continuous phase was not changed in this study, the capillary number remained constant, and the size of the MB was only affected by the ratio between the continuous and dispersed flow rates. For example, when the flow rate of the dispersed phase is too low, the lower limit of the flow rate of the continuous phase decreases to reach the same diameter as the QD-MBs. However, at higher continuous flow velocities, the flow pattern changed from dripping to reflux. However, if the flow rate of the dispersed phase is too high, the flow pattern changes from elongation to jetting and is not suitable for the production of QD-MBs. These observations show that the flow pattern can affect the size of the beads; however, the best method for producing stable monodisperse beads is dripping. This method produces homogeneous spherical beads that can be controlled by adjusting the flow rate.

QD-MBs have great potential for use in various biosensing, imaging, and drug delivery applications.[5,17,30,52] In particular, QD-MBs can be functionalized with specific ligands or antibodies that enable precise binding to biological targets, facilitating their application in biosensing and diagnostics.[18,53,54] In addition, the inherent porosity of MBs enables the encapsulation and controlled release of drugs or other therapeutic agents, making them potential candidates for advanced drug delivery systems.[55] This study presents a facile method to fabricate monodispersed QD-MBs of various sizes, with potential importance in important fields such as biomedicine and materials science.

Conclusions

In conclusion, we developed a simple microfluidic method for the synthesis of monodisperse QD-MBs with controllable sizes using a specially designed QD-PR. The QD-MBs were characterized using fluorescence microscopy, and their size distribution and FWHM were analyzed. We demonstrated that the QD-MBs have a uniform and spherical shape with uniform emission, and that their size can be easily controlled by adjusting the flow rates of the continuous and dispersed phases during fabrication. Moreover, the QD-MBs exhibited a narrower FWHM than their colloidal QD counterparts, showing a more uniform distribution and higher density of QDs within the MB structure. In previous studies, we showed a uniform distribution of QDs in a cured super-coater, suggesting that this uniformity could be maintained in QD-MBs with the same material. We aimed to develop a simple and effective method for fabricating monodisperse and uniform QD-MBs using microfluidics. We also investigated numerous factors affecting the fabrication process and optimized them accordingly. However, further studies are needed to clarify the exact interplay between the QD dispersion and QY in QD-MBs. Overall, the method presented in this study provides a simple and efficient approach for the fabrication of size-controllable QD-MBs, which could be important for many applications, such as biosensing, drug delivery, and imaging. Further optimization of the method could lead to the fabrication of QD-MBs with even narrower size distributions and improved optical properties, as well as the incorporation of other functional materials into MBs for more diverse applications.

Author contributions

Conceptualization, S. O. K., S. S.; investigation, B. K., B. C.; data curation, B. K., S. K., B. C.; formal analysis, B. K., S. K., S. S.; visualization, B. K., S. K., S. S.; methodology, B. K., S. K., S. S.; writing – original draft, B. K., S. K.; writing – review and editing, B. K., S. K., H. S., S. O. K., S. S.; writing – final draft, H. S., S. O. K., S. S.; supervision, H. S., S. O. K., S. S.; project administration, H. S., S. O. K., S. S.; funding acquisition, S. O. K., S. S.

Conflicts of interest

There are no conflicts to declare.

Acknowledgements

This study was supported by the Basic Science Research Program of the National Research Foundation (NRF) of Korea (Grant#: 2020R1A2C1012109), the Korea Medical Device Development Fund funded by the Korean Government (Ministry of Science and ICT; Ministry of Trade, Industry, and Energy; Ministry of Health & Welfare; Ministry of Food and Drug Safety) (Grant#: RS-2020-KD000142), the International Science & Business Belt support program through the Korea Innovation Foundation funded by the Ministry of Science and ICT (MSIT) (Grant#: 2023-SB-SB-0019), the Information

Technology Research Center (ITRC) support program supervised by the IITP (Institute for Information & Communications Technology Planning & Evaluation) and funded by the Ministry of Science and ICT (MSIT), Korea (Grant#: IITP-2023-RS-2023-00258971), and the Korea Institute of Marine Science & Technology Promotion (KIMST) support program funded by the Ministry of Oceans and Fisheries, Korea (Grant#: 20210660).

References

1 A. P. F. Turner, *Chem. Soc. Rev.*, 2013, **42**, 3184–3196.
2 J. Kim, A. S. Campbell, B. E.-F. De Ávila and J. Wang, *Nat. Biotechnol.*, 2019, **37**, 389–406.
3 M. Roy, G. Jin, J.-H. Pan, D. Seo, Y. Hwang, S. Oh, M. Lee, Y. J. Kim and S. Seo, *Sens. Actuators, B*, 2016, **224**, 577–583.
4 Q. Guo, F. Bian, Y. Liu, X. Qu, X. Hu and Q. Sun, *Chem. Commun.*, 2017, **53**, 4954–4957.
5 B.-H. Jun, H. Kang, Y.-S. Lee and D. H. Jeong, *Molecules*, 2012, **17**, 2474–2490.
6 I. V. Martynenko, D. Kusić, F. Weigert, S. Stafford, F. C. Donnelly, R. Evstigneev, Y. Gromova, A. V. Baranov, B. Rühle, H.-J. Kunte, Y. K. Gun'ko and U. Resch-Genger, *Anal. Chem.*, 2019, **91**, 12661–12669.
7 N. Sun, X. Li, Z. Wang, Y. Li and R. Pei, *Biosens. Bioelectron.*, 2018, **102**, 157–163.
8 B. Ortiz-Casas, A. Galdámez-Martínez, J. Gutiérrez-Flores, A. Baca Ibañez, P. Kumar Panda, G. Santana, H. A. de la Vega, M. Suar, C. Gutiérrez Rodelo, A. Kaushik, Y. Kumar Mishra and A. Dutt, *Mater. Today*, 2021, **50**, 533–569.
9 A. Jo, T. H. Kim, D.-M. Kim, H.-M. Kim, B. Seong, J. Kim, X.-H. Pham, H. S. Jung, S. H. Lee, D. W. Hwang, D. H. Jeong, Y.-S. Lee, D.-E. Kim and B.-H. Jun, *J. Ind. Eng. Chem.*, 2020, **90**, 319–326.
10 Q. Song, X. Sun, Z. Dai, Y. Gao, X. Gong, B. Zhou, J. Wu and W. Wen, *Lab Chip*, 2021, **21**, 1634–1660.
11 M. Byakodi, N. S. Shrikrishna, R. Sharma, S. Bhansali, Y. Mishra, A. Kaushik and S. Gandhi, *Biosens. Bioelectron.: X*, 2022, **12**, 100284.
12 K. Tabata, D. Braam, S. Kushida, L. Tong, J. Kuwabara, T. Kanbara, A. Beckel, A. Lorke and Y. Yamamoto, *Sci. Rep.*, 2014, **4**, 5902.
13 L. Wei, S. Yan, H. Wang and H. Yang, *NPG Asia Mater.*, 2018, **10**, 899–911.
14 N. Sankova, P. Shalaev, V. Semeykina, S. Dolgushin, E. Odintsova and E. Parkhomchuk, *J. Appl. Polym. Sci.*, 2021, **138**, 49890.
15 I. F. Pinto, C. R. F. Caneira, R. R. G. Soares, N. Madaboosi, M. R. Aires-Barros, J. P. Conde, A. M. Azevedo and V. Chu, *Methods*, 2017, **116**, 112–124.
16 H. Yabu, *Part. Part. Syst. Charact.*, 2019, **36**, 1900178.
17 L. Scholtz, J. G. Eckert, T. Elahi, F. Lübkemann, O. Hübner, N. C. Bigall and U. Resch-Genger, *Sci. Rep.*, 2022, **12**, 12061.
18 A. Vafajoo, A. Rostami, S. Foroutan Parsa, R. Salarian, N. Rabiee, G. Rabiee, M. Rabiee, M. Tahriri, D. Vashaee, L. Tayebi and M. R. Hamblin, *Biomed. Microdevices*, 2018, **20**, 66.
19 E. Hemmer, N. Venkatachalam, H. Hyodo, A. Hattori, Y. Ebina, H. Kishimoto and K. Soga, *Nanoscale*, 2013, **5**, 11339–11361.
20 U. Resch-Genger, M. Grabolle, S. Cavaliere-Jaricot, R. Nitschke and T. Nann, *Nat. Methods*, 2008, **5**, 763–775.
21 K. D. Wegner and N. Hildebrandt, *Chem. Soc. Rev.*, 2015, **44**, 4792–4834.
22 V. Singh, Priyanka, P. V. More, E. Hemmer, Y. K. Mishra and P. K. Khanna, *Mater. Adv.*, 2021, **2**, 1204–1228.
23 A. A. Jadhav, P. V. More and P. K. Khanna, *RSC Adv.*, 2015, **5**, 76733–76742.
24 J. Zhang, S. Shikha, Q. Mei, J. Liu and Y. Zhang, *Mikrochim. Acta*, 2019, **186**, 361.
25 E. M. Rodrigues, N. D. Calvert, J. C. Crawford, N. Liu, A. J. Shuhendler and E. Hemmer, *Small*, 2022, **18**, e2107130.
26 H. Li, B. Dong, L. Dou, W. Yu, X. Yu, K. Wen, Y. Ke, J. Shen and Z. Wang, *Sens. Actuators, B*, 2020, **324**, 128771.
27 Y. Wei, X. Deng, Z. Xie, X. Cai, S. Liang, P. Ma, Z. Hou, Z. Cheng and J. Lin, *Adv. Funct. Mater.*, 2017, **27**, 1703535.
28 M. Kuang, D. Wang, H. Bao, M. Gao, H. Möhwald and M. Jiang, *Adv. Mater.*, 2005, **17**, 267–270.
29 Q. He, X. Chen, Y. He, T. Guan, G. Feng, B. Lu, B. Wang, X. Zhou, L. Hu and D. Cao, *Biosens. Bioelectron.*, 2019, **129**, 107–117.
30 K. Brazhnik, Z. Sokolova, M. Baryshnikova, R. Bilan, A. Efimov, I. Nabiev and A. Sukhanova, *Nanomedicine*, 2015, **11**, 1065–1075.
31 W. Yin, H. Liu, M. Z. Yates, H. Du, F. Jiang, L. Guo and T. D. Krauss, *Chem. Mater.*, 2007, **19**, 2930–2936.
32 J. Tan, G. Zhao, Z. Zeng and M. A. Winnik, *Macromolecules*, 2015, **48**, 3629–3640.
33 K.-H. Kim, P. H. Dannenberg, H. Yan, S. Cho and S.-H. Yun, *Adv. Funct. Mater.*, 2021, **31**, 2103413.
34 S. Shikha, X. Zheng and Y. Zhang, *Nano-Micro Lett.*, 2018, **10**, 31.
35 X. Luo, P. Su, W. Zhang and C. L. Raston, *Adv. Mater. Technol.*, 2019, **4**, 1900488.
36 G. M. Whitesides, *Nature*, 2006, **442**, 368–373.
37 Y. H. Roh, H. J. Lee and K. W. Bong, *BioChip J.*, 2019, **13**, 64–81.
38 Y. Cheng, S. D. Ling, Y. Geng, Y. Wang and J. Xu, *Nanoscale Adv.*, 2021, **3**, 2180–2195.
39 E. K. Sackmann, A. L. Fulton and D. J. Beebe, *Nature*, 2014, **507**, 181–189.
40 K. S. Elvira, X. Casadevall i Solvas, R. C. R. Wootton and A. J. deMello, *Nat. Chem.*, 2013, **5**, 905–915.
41 F. Montanarella, D. Urbonas, L. Chadwick, P. G. Moerman, P. J. Baesjou, R. F. Mahrt, A. van Blaaderen, T. Stöferle and D. Vanmaekelbergh, *ACS Nano*, 2018, **12**, 12788–12794.
42 M. D. Eqbal, F. Naaz, K. Sharma and V. Gundabala, *Colloids Surf., B*, 2021, **208**, 112065.

43 Y. Jeong, H. Jang, J. Kang, J. Nam, K. Shin, S. Kwon and J. Choi, *Biosensors*, 2021, **11**, 283.
44 M. Rabiee, N. Namaei Ghasemnia, N. Rabiee and M. Bagherzadeh, in *Biomedical Applications of Microfluidic Devices*, Elsevier, 2021, pp. 153–186.
45 H. Liu, G. Li, X. Sun, Y. He, S. Sun and H. Ma, *RSC Adv.*, 2015, **5**, 62706–62712.
46 S. Myeong, B. Chon, S. Kumar, H.-J. Son, S. O. Kang and S. Seo, *Nanoscale Adv.*, 2022, **4**, 1080–1087.
47 C. T. Rueden, J. Schindelin, M. C. Hiner, B. E. DeZonia, A. E. Walter, E. T. Arena and K. W. Eliceiri, *BMC Bioinf.*, 2017, **18**, 529.
48 K. R. Choudhury, Y. Sahoo, T. Y. Ohulchanskyy and P. N. Prasad, *Appl. Phys. Lett.*, 2005, **87**, 073110.
49 J. K. Nunes, S. S. H. Tsai, J. Wan and H. A. Stone, *J. Phys. D: Appl. Phys.*, 2013, **46**, 114002.
50 D.-Y. Kim, S. H. Jin, S.-G. Jeong, B. Lee, K.-K. Kang and C.-S. Lee, *Sci. Rep.*, 2018, **8**, 8525.
51 K.-K. Kang, B. Lee and C.-S. Lee, *Microelectron. Eng.*, 2018, **199**, 1–15.
52 S. W. Ahn, M. Ko, S. Yoon, J. H. Oh, Y. Yang, S. H. Kim, J. K. Song and Y. R. Do, *ACS Appl. Nano Mater.*, 2022, **5**, 16070–16081.
53 S. F. Parsa, A. Vafajoo, A. Rostami, R. Salarian, M. Rabiee, N. Rabiee, G. Rabiee, M. Tahriri, A. Yadegari, D. Vashaee, L. Tayebi and M. R. Hamblin, *Anal. Chim. Acta*, 2018, **1032**, 1–17.
54 Q. Jin, X. Zhang, L. Zhang, J. Li, Y. Lv, N. Li, L. Wang, R. Wu and L. S. Li, *Inorg. Chem.*, 2023, **62**, 3474–3484.
55 R. Gui, Y. Wang and J. Sun, *Colloids Surf., B*, 2014, **113**, 1–9.